Initiation of Boreal Summer Intraseasonal Oscillation: Dynamic Contribution by Potential Vorticity

KYONG-HWAN SEO AND EUN-JI SONG

Department of Atmospheric Sciences, Division of Earth Environmental System, Pusan National University, Busan, South Korea

(Manuscript received 27 April 2011, in final form 23 September 2011)

ABSTRACT

Potential vorticity (PV) thinking conceptually connects the upper-level (upper troposphere in the extratropics and middle troposphere for the tropics) dynamical process to the lower-level process. Here, the initiation mechanism of the boreal summer intraseasonal oscillation (BSISO) in the tropics is investigated using PV thinking. The authors demonstrate that the midtropospheric PV anomaly produces a dynamical environment favorable for the BSISO initiation. Under seasonal easterly vertical wind shear, the PV anomaly enhances low-level convergence and upward motion at its western edge. Tropical PV forcing in the middle troposphere produces balanced mass and circulation fields that spread horizontally and vertically so that its effect can reach even the lowest troposphere. The downward influence of the midtropospheric PV forcing is one of the key aspects of the PV thinking. Direct piecewise PV inversions confirm that the anomalous lower-level zonal wind and its convergence necessary for the initiation of BSISO convection do not arise solely from the response to the lower-level PV forcing but from the summed contribution by PV forcing at all levels. About 50% of the low-level circulation variations result from PV forcing from 700 to 450 hPa, with the largest contribution from the 600–650-hPa PV anomalies for the convection initiation region over the western Indian Ocean. The current study is compared with and incorporated into the thermodynamic recharge process and the frictional moisture flux convergence mechanism for the BSISO initiation. This study is the first qualitative application of the PV thinking approach that reveals the BSISO dynamics.

1. Introduction

The Madden–Julian oscillation (MJO) or intraseasonal oscillation (ISO) is the most dominant subseasonal mode in the tropics (Madden and Julian 1994). Although the boreal winter MJO exhibits strong eastward propagation along the equator from the Indian Ocean to the date line, its summer counterpart, referred to as the boreal summer intraseasonal oscillation (BSISO) shows a complex propagation pattern due to prominent northward propagation associated with the Asian monsoon over the Indian Ocean and the western Pacific, as well as the formation of the summertime intertropical convergence zone off the equator (Sikka and Gadgil 1980; Lau and Chan 1986; Wang and Rui 1990; Annamalai and Sperber 2005; Seo et al. 2007; and others). The northwestward-propagating BSISO in the East Asian monsoon region is also known to be a major factor in the active and break phases of the rainy spells during the summer season (e.g., Yun et al. 2008). Among the many unresolved physical mechanisms associated with the BSISO (and, more comprehensively, the MJO), the initiation mechanisms remain elusive. Proposed theories on the initiation processes of the BSISO (or the MJO) can be categorized into the following three types: the internal (tropical) dynamics mechanism (including upstream Kelvin wave forcing, a discharge–recharge process, and a low-level wind convergence mechanism), the external (extratropics) dynamics mechanism, and the stochastic forcing mechanism.

New MJO convection can be generated over the western equatorial Indian Ocean (WEIO) by a circumnavigating Kelvin wave induced by the previous cycle of MJO convection (Hendon 1988; Bladé and Hartmann 1993), by a Kelvin wave forced by an enhanced heating anomaly over western Africa (Hsu and Lee 2005), or by a Rossby wave response to the suppressed convection over the eastern equatorial Indian Ocean (EEIO) (Matthews 2000; Seo and Kim 2003; Hsu and Lee 2005; Jiang and Li 2005). Seo and Kim (2003) showed that both the encircling

Corresponding author address: Dr. Kyong-Hwan Seo, Department of Atmospheric Sciences, Pusan National University, Busan, South Korea.
E-mail: khseo@pusan.ac.kr

DOI: 10.1175/MWR-D-11-00105.1

Kelvin wave generated by enhanced convection of the previous cycle and the Rossby wave generated by reduced convection of the current cycle over the Indian Ocean appear to generate a new convection over the WEIO.

Recently, the discharge–recharge hypothesis for the life cycle of the MJO (Bladé and Hartmann 1993), in which the initiation and period of the oscillation are determined by the local oscillation of recharge and discharge of convective instability, has been receiving increasing attention. Kemball-Cook and Weare (2001), Benedict and Randall (2007), and Thayer-Calder and Randall (2009) presented observational evidence to support this hypothesis. They showed that anomalous, sufficient low-level heating and moistening by shallow convection prior to peak convection is considered to be a key process for the later development of a deep MJO convective event (see also Seo and Wang 2010).

The low-level moisture convergence caused by anomalous winds develop as a Rossby wave response to suppressed convection over the equatorial central or eastern Indian Ocean related to the previous break phase of the BSISO. Annamalai and Sperber (2005), using linear models, proposed that this convergence is the major agent triggering the next active phase of the BSISO over the WEIO. In addition, Hsu and Lee (2005) showed that the lifting and frictional effects of tropical African topography enhance the low-level moisture convergence over the WEIO. Similarly, a recent study by Matthews (2008) suggested the presence of suppressed convection prior to the beginning of enhanced convection over the Indian Ocean in both successive and single primary Madden–Julian events, and it was conjectured that, in these events, the low-level circulation anomalies associated with suppressed convection help in forming the next enhanced cycle. However, this process was not explicitly considered in the study conducted by Matthews. On the other hand, the horizontal temperature advection in the tropical Indian Ocean has been proposed as the main factor in initiating BSISO convection. For example, Jiang and Li (2005) attributed the low-level convergence over the WEIO, which is considered to be a major driver for a new convection over the WEIO, to the mean temperature gradient advection by the BSISO meridional wind and the perturbation temperature gradient advection by the mean meridional flow, rather than the weakening of easterly zonal flow to the west of the suppressed convection (which signifies the western equatorial behavior of the Rossby wave response to suppressed convection over the central–eastern Indian Ocean). This hypothesis implies a self-sustained process for the BSISO in the tropical Indian Ocean and is thus consistent with the view that the BSISO is a basinwide Indian Ocean mode.

The external dynamics mechanism is associated with the propagation of the upper-tropospheric Rossby wave train, wherein its energy dispersion from extratropics to the tropical Indian Ocean might trigger the initiation of the MJO (Hsu et al. 1990; Bladé and Hartmann 1993; Slingo 1998; Matthews and Kiladis 1999; Lin et al. 2000). Recently, using a wave activity flux vector for the detection of the source and propagation of waves, Ray and Zhang (2010) showed some evidence of an extratropical influence. In their study, latitudinal momentum transport from the Southern Hemisphere extratropics to the tropical Indian Ocean is shown to play a crucial role in generating the tropical lower-tropospheric westerlies that lead to the MJO initiation. The result from a simple dry atmospheric model run by Lin et al. (2007) also exhibited a strong extratropical influence with a southward wave activity flux from the North Atlantic to the tropics and later to the equatorial Indian Ocean in the form of Kelvin waves. Interestingly, Matthews (2008) showed that enhanced transient Rossby wave activity measured by the kinetic energy of the high-frequency (20-day high-pass filtered) upper-level wind anomalies is observed between 10° and 30°N and leads equatorial convection for successive MJO events over the African and Indian Ocean sectors.

The stochastic forcing mechanism is related to the high-frequency variability in tropical convective processes and extratropical disturbances that produce the large-scale variability of equatorial waves. A more detailed explanation or review of these hypotheses can be found in Matthews (2000), Seo and Kim (2003), Hsu et al. (2004), Zhang (2005), Jiang and Li (2005), Lin et al. (2007), and Ray et al. (2009). The objective of this study is to investigate further the initiation mechanism of the BSISO using a potential vorticity (PV) framework (Hoskins et al. 1985; Bluestein 1993, 180–219).

As mentioned above, the internally induced initiation mechanisms are largely confined to the lower-tropospheric thermodynamic and dynamical processes. For example, in the discharge–recharge hypothesis, preconditioning of the moisture and temperature in the lower troposphere is required for the development of deep convection, and thus it serves as a thermodynamic precursory feature. In addition, the lower-level moisture convergence over the WEIO caused by the Rossby wave response to the convective event of the opposite sign in the EEIO and the upstream Kelvin wave effect are considered to be dynamical precursory processes. However, in this study, we utilize the middle- and lower-tropospheric dynamic signature for the initiation of a new BSISO convection over the Indian Ocean. Consisting of relative vorticity, planetary vorticity, and vertical static stability, PV reflects both dynamic (vorticity) and thermodynamic

(vertical stability of the air) properties in the atmosphere. It is conserved following frictionless and adiabatic motions and essentially related to the spatial structures of wind and temperature fields. The PV thinking, characterized by use of PV conservation and invertibility principles for understanding atmospheric dynamics and the evolution of large-scale atmospheric systems, is introduced in this study, and this conceptually connects the upper-level (upper troposphere and lower stratosphere in the extratropics and middle troposphere for the tropics; so here it is referred to the middle troposphere) dynamical process to the lower-tropospheric process. In particular, PV invertibility provides the spatial structures of wind and mass fields consistent with the PV anomalies, making it possible to estimate quantitatively the effect of the higher-level PV anomalies on the lower-tropospheric mass and wind variations. We demonstrate that the midtropospheric PV anomaly plays an important role in the BSISO initiation that begins to develop in the lower layer.

Only a few papers have presented the role of PV on the initiation of tropical convection in general or that associated with the MJO. Matthews et al. (1996) revealed that PV advection due to the subtropical Rossby wave response plays a role in the poleward and eastward propagation of MJO convection along the South Pacific convergence zone. Based on a case study, Allen et al. (2009) recently showed that the modulation of tropical convection is closely linked to a series of breaking Rossby wave activities on the southern subtropical jet and subsequent extension into the tropics. A convective event develops at the leading edge of a PV entity (which corresponds to a sharp boundary between moist and dry air), whereas convection is inhibited beneath the vicinity of PV anomaly center.

In this study, we first present some observational characteristics of the PV anomaly associated with the BSISO. Next, the initiation mechanism of the BSISO is presented in terms of PV thinking. Datasets and the methods used in this study are described in section 2. In section 3, a PV inversion and the initiation mechanism are suggested. In section 4, the results of this study are compared with and incorporated into the previously proposed initiation theories. Finally, the summary is given in section 5.

2. Data and methodology

a. Data

The daily outgoing longwave radiation (OLR) data obtained from the Advanced Very High Resolution Radiometer (AVHRR) onboard the National Oceanic and Atmospheric Administration (NOAA) polar-orbiting satellites for the period of 1979–2001 (23 yr) are used as a proxy of the deep convection of the BSISO. To represent the dynamical and moisture variations associated with the BSISO, the 40-yr European Centre for Medium-Range Weather Forecasts (ECMWF) Re-Analysis (ERA-40) dataset is utilized for the same 23-yr period. Previous studies (Lin and Johnson 1996; Straub and Kiladis 2003) suggested that ERA-40 data are comparable to the data from the Tropical Ocean Global Atmosphere Coupled Ocean–Atmosphere Response Experiment (TOGA COARE).

All these datasets are on a 2.5° by 2.5° longitude–latitude grid. The analysis season is the extended boreal summer defined as the 5-month period from 1 May to 30 September. The anomalies are derived by removing the annual cycle composed of the time mean and the first three annual harmonics at each grid point. To isolate the 25–80-day BSISO signal, a Lanczos filter (Duchon 1979) with 141 weights is applied to the anomaly data.

b. Methodology

In this study, PV on an isobaric coordinate is diagnosed. Three main reasons can be listed for avoiding an isentropic PV analysis: 1) the existence of strong diabatic heating and updraft across isentropic surfaces over the tropics, 2) the feasibility in the comparison of the documented BSISO (or MJO) diagnostics at pressure levels (e.g., Zhang and Ling 2012), and 3) the easier application of boundary conditions for PV inversion (e.g., Kim et al. 2009). Because the vertical component of absolute vorticity and the vertical gradient of potential temperature θ are dominant compared to other components, isobaric PV can be written as

$$\mathrm{PV} \cong -g(f + \zeta)\frac{\partial \theta}{\partial p}, \tag{1}$$

where f is the Coriolis parameter, ζ is the vertical component of relative vorticity, and g is the gravitational acceleration.

As explained in the introduction, three-dimensional PV distribution produces temperature and wind fields that are balanced with the PV distribution through a PV inversion technique (e.g., Hoskins et al. 1985; Davis and Emanuel 1991; Davis 1992). This inversion is done by utilizing the constraints for large-scale motions such as geostrophic and hydrostatic relations. Imposing proper boundary conditions produces unique solutions. In the isobaric coordinate, PV in (1) can be expressed as the spatial distributions of streamfunction and geopotential height through the Exner function, $\Pi = c_p(p/p_0)^{c_p/R_d}$, where c_p is the heat capacity of dry air at constant

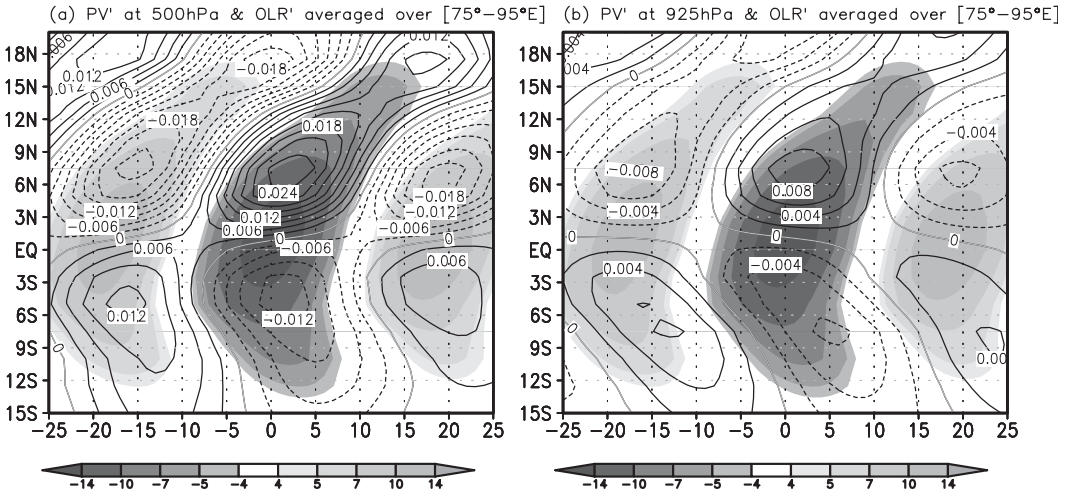

FIG. 1. Time–latitude plot of PV anomalies (contours) and OLR anomalies (shading) regressed onto the OLR time series index for the base region over the equatorial Indian Ocean (5°S–5°N, 75°–95°E): (a) 500 and (b) 925 hPa. Intervals of OLR are shown in the gray scale bar, and those for PV at 500 and 925 hPa are 0.3×10^{-2} and 0.2×10^{-2} PV units (PVU, 1 PVU = 10^{-6} K m^2 kg^{-1} s^{-1}), respectively. The shaded and contoured anomalies (excluding zero contours) are significant at the 90% confidence level.

pressure; p is the pressure and p_0 is the pressure at the reference level, usually taken as 1000 hPa; and R_d is the gas constant for dry air. As the upper and lower boundary conditions for PV inversion, potential temperature anomaly fields are specified to be zero at these two levels. Detailed inversion procedures and related equations are omitted in this study, but readers can refer to Davis and Emanuel (1991) and Davis (1992) or elsewhere. These derived geopotential height and streamfunction fields consistent with the midtropospheric PV anomalies spread horizontally and vertically so that these anomalies can reach even the lowest troposphere. The downward influence of the upper-level PV is one of the key aspects of the PV thinking.

To determine the general characteristics associated with the BSISO, conventional lead–lag regression is applied to the anomalies of PV, OLR, and the other dynamical variables. The index time series used in this study is the normalized time series of OLR anomalies averaged over the central–eastern Indian Ocean (5°S–5°N, 75°–95°E), where the intraseasonal variance is locally maximized (not shown) (e.g., Seo and Kumar 2008). A standard deviation of 16.1 W m^{-2} is used for this normalization, and this index time series will be hereafter referred to as the OLR index. For a statistical significance test, Student's t test is applied using the effective degree of freedom estimated by the method suggested by Ebisuzaki (1997), $N_{\text{eff}} = N\left[\sum_{\tau=-N+1}^{N-1}(1 - |\tau|/N)\rho_{\text{AA}}(\tau)\rho_{\text{BB}}(\tau)\right]^{-1}$, where ρ_{AA} and ρ_{BB} are the autocorrelation of two variables (e.g., the OLR index and the PV anomaly), N is the total data length, and τ denotes lag. According to this method, the characteristic time scale is estimated to be approximately 17 days.

3. Results

a. Observed feature of the PV anomaly

Because PV is proportional to absolute vorticity and static stability, it is very useful in understanding the generation of vorticity in relation to cyclogenesis, especially along the polar front. In addition, the PV approach has been applied to the study of tropical cyclones. For example, Nong and Emanuel (2003) examined the contribution of an upper-level moist PV anomaly to the genesis of concentric eyewalls in hurricanes. Following the initial presentation by Hoskins et al. (1985), PV thinking has become useful in synoptic analysis. However, no study has been conducted on the relevance of PV thinking to the BSISO; this forms the focus of the current study. Note that the effective penetration depth of PV influence is proportional to the Rossby ratio and horizontal scale of PV entity considered. The estimated downward penetration depth is about 5–6 km in the tropics so that the midtropospheric PV anomaly is able to affect the lower-level circulation feature.

Figure 1 shows the time–latitude cross section of the PV anomalies (contour) at 500 (middle troposphere) and 925 hPa (lower troposphere) and OLR anomalies (shading) regressed onto the OLR time series index for the equatorial central–eastern Indian Ocean base region. Here, lag day 0 indicates the time of occurrence of the greatest convection intensity in the base domain.

The dipole PV anomalies appear off the equator in association with the suppressed and enhanced convection. The middle- and lower-level PV anomalies to the north and south of the convection clearly develop as a Rossby wave response to the convection (Wang and Xie 1997; Kemball-Cook and Wang 2001). The PV anomalies exhibit a barotropic vertical structure due to the barotropic development of relative vorticity anomalies in the tropics. After day −5, when the convection reaches the central–eastern Indian Ocean, the northward propagation of the convection and positive PV anomalies is apparent.

Figure 2 shows the time evolution of horizontal 500-hPa PV (contour) and OLR (shading) anomalies. This time sequence, centered at the BSISO initiation phase of day −13, encompasses the life cycle from the development of suppressed convection and subsequent enhanced convection over the Indian Ocean to its northward shift at a later stage. During the suppressed convection phase (from day −30 to day −15), negative and positive PV anomalies are generated to the north and south of the suppressed convection center in response to the suppressed convection, respectively. By day −13, enhanced convection (blue color) begins to develop along the equator over the western Indian Ocean. In fact, this is situated at the left edge of the positive PV pool over the equatorial central–eastern Indian Ocean. Later in this paper, we interpret this development of the enhanced convection on day −13 in terms of PV thinking and show that the positive PV anomaly generated from the previous suppressed convection helps induce the opposite phase of the upstream convective event. After that, the suppressed convection breaks up into the two entities, both exhibiting Rossby wave characteristics. The northern one continues to propagate to the north, but the southern one decays with time because of the easterly vertical shear of background climatological zonal wind (Wang and Xie 1997; Seo et al. 2007). The suppressed convection over the Indian subcontinent, the South China Sea, and the equatorial western Pacific forms a tilted structure, which is a well-known feature associated with the BSISO.

b. *Relationships between PV and other meteorological variables and PV thinking*

The preceding section examined the PV distribution consistent with the evolution of the BSISO convection. In this section, the horizontal and vertical distributions of other dynamic variables are presented, and a dynamic connection among these is investigated using a PV thinking approach. First, Fig. 3 shows OLR, 925-hPa moisture convergence, and 500-hPa vertical velocity anomalies regressed onto the OLR index at the phase of initiation (day −13). As stated above, enhanced convection (blue) develops at the western edge of the PV anomaly over the Indian Ocean (Fig. 3a). Under this PV anomaly, low-level moisture convergence (Fig. 3b) and negative pressure velocity (Fig. 3c) are collocated. Figure 4 shows the longitude–height cross sections of PV, pressure velocity, wind convergence anomalies, and climatological mean zonal wind on day −13 at 5°S, where the convection initiates. An equivalent barotropic structure in PV anomalies is seen over the central Indian Ocean with the peak axis slightly tilted toward the west (Fig. 4a). The amplitude of the regressed positive PV anomaly increases with height due to stronger static stability near the tropopause. The anomalous low-level wind convergence and divergence appear to the west and east of the PV anomaly, over 40°E and 90°–105°E, respectively (Fig. 4c). A weaker convergence zone is also formed in between. The leftmost convergence zone corresponds to the left edge of the 500-hPa PV anomaly, which has been proposed to be a main convection promotion region (Allen et al. 2009). By continuity, an upward and downward motion to the west and east of the 500-hPa PV anomaly center develop (Fig. 4a), showing that the induced low-level convergence and upward motion are related to the relative location to the PV anomaly.

This phasing between the midtropospheric PV and low-convergence and vertical motion anomalies during the initiation process can be explained by the PV thinking approach under the seasonal mean easterly vertical wind shear (Fig. 4b). A schematic plot for aiding this explanation is presented in Fig. 5. During boreal summer, the observed climatological basic zonal winds are westerlies at the lower level and easterlies at the middle and upper levels (in Fig. 4b and denoted as open arrows on the right side in Fig. 5). In the reference frame moving with the positive PV anomaly at the middle or upper level, the anomaly at this level is stationary. However, due to the vertical shear, a westerly flow occurs at the lower level (open arrows on the left side) (Bluestein 1993, 180–219). Therefore, the westerly relative basic wind tries to transport a counterclockwise vortex at the lower level, which is induced by the positive PV anomaly aloft, to the east, so that positive vorticity advection (PVA) and negative vorticity advection (NVA) areas appear to the right and left sides of the induced counterclockwise vortex, respectively. According to the vorticity equation (Holton 2004, 108–111):

$$\frac{\partial(\zeta + f)}{\partial t} = -\mathbf{V}\cdot\nabla(\zeta + f) - (\zeta + f)\nabla\cdot\mathbf{V} - \omega\frac{\partial\zeta}{\partial p} + \mathbf{k}\cdot\left(\frac{\partial\mathbf{V}}{\partial p}\times\nabla\omega\right), \quad (2)$$

where the definitions of the variables follow their usual meaning or convention in atmospheric sciences. The left

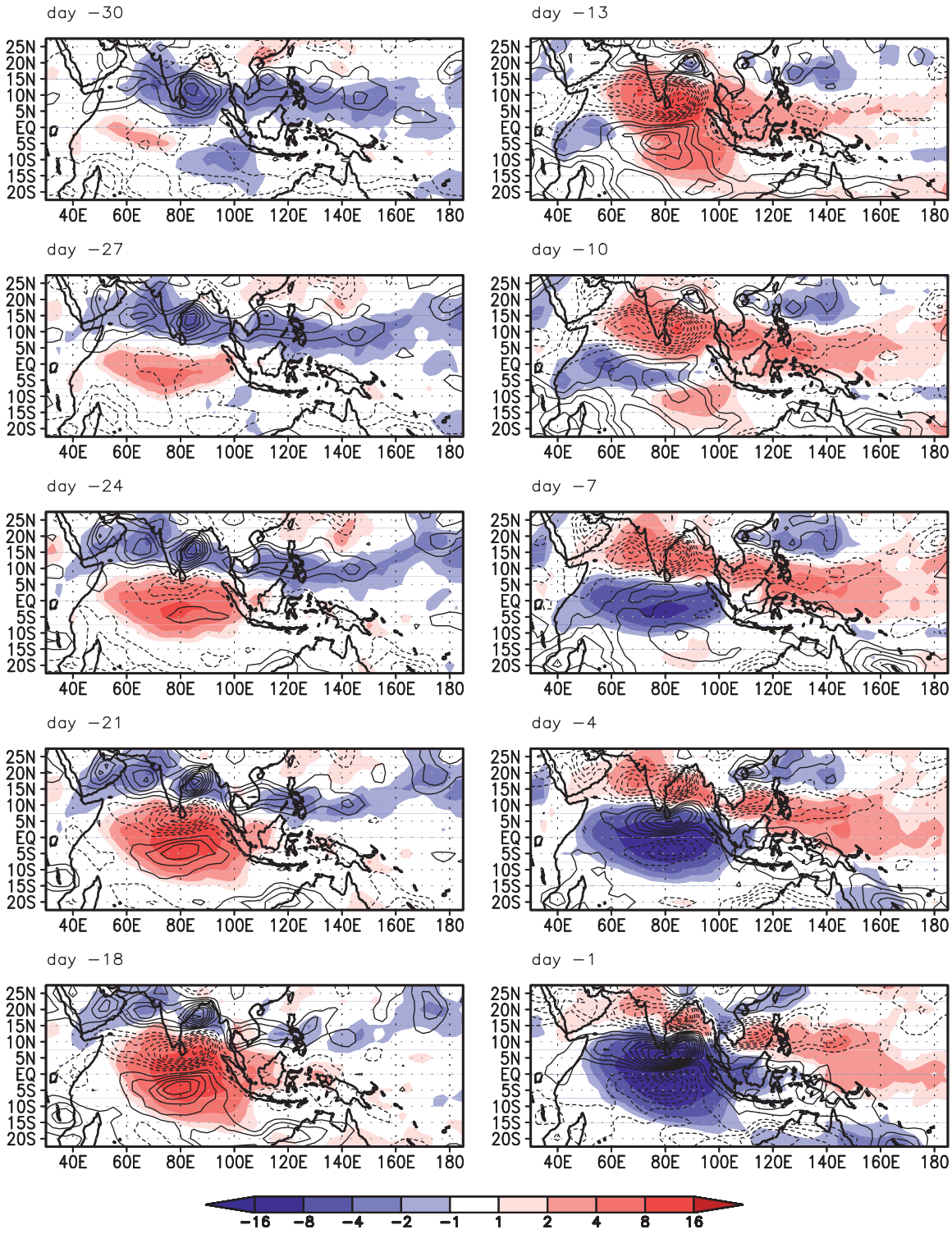

FIG. 2. Time evolution of 500-hPa PV (contours) and OLR (shading) anomalies from day −30 to −1 (i.e., from the suppressed convection phase to the enhanced convection phase over the Indian Ocean). The contour interval of PV is 0.3×10^{-2} PVU, and that for OLR is shown in the color bar (in units of W m^{-2}). The solid (dashed) lines denote the positive or counterclockwise (negative or clockwise) PV anomalies. The shaded and contoured anomalies are significant at the 90% confidence level.

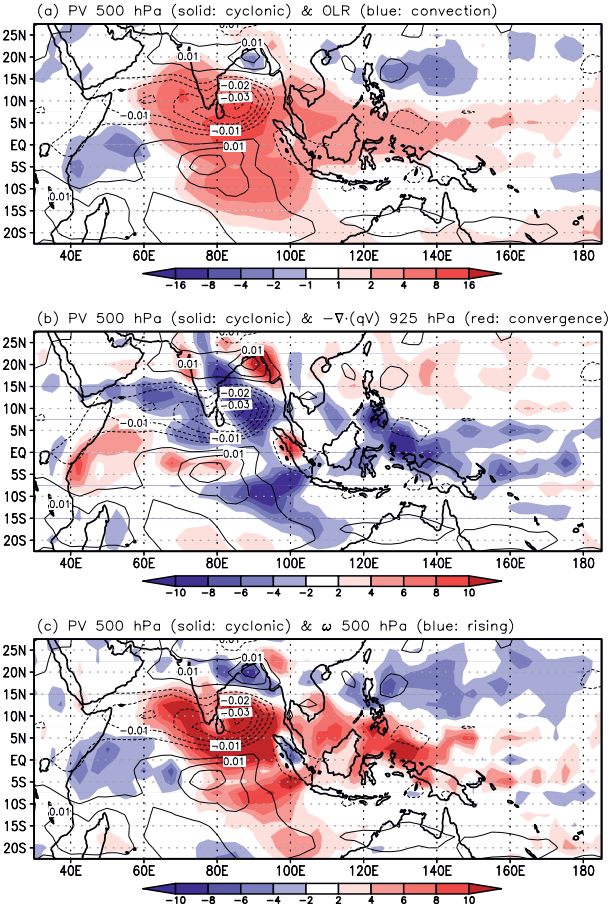

FIG. 3. Day −13 horizontal distribution of 500-hPa PV (contours) and (a) OLR (shading), (b) moisture convergence at 925 hPa (shading), and (c) vertical velocity at 500 hPa (shading) regressed onto the OLR index. The interval information of PV and OLR is as in Fig. 1. The intervals of 925-hPa moisture convergence and 500-hPa vertical velocity are 2×10^{-6} s^{-1} and 2×10^{-3} hPa s^{-1}, respectively. The shaded anomalies are significant at the 90% confidence level.

term is the time rate of absolute vorticity, and the terms on the right-hand side are the horizontal advection of absolute vorticity, horizontal convergence, vertical advection of relative vorticity, and tilting, respectively. Because absolute vorticity in the reference frame of the positive PV anomaly does not change even below where the induced wind fields extend (see Bluestein 1993, 180–219) and the first two terms on the right-hand side are more than one order greater than the third and fourth terms over the Indian Ocean, the equation can be expressed as

$$0 \cong -\mathbf{V} \cdot \nabla(\zeta + f) - (\zeta + f)\nabla \cdot \mathbf{V}. \qquad (3)$$

This means that the region on the west of the PV anomaly, which is the NVA region, undergoes horizontal convergence, whereas the PVA region on the east of the PV anomaly should be balanced with the horizontal divergence. The continuity consideration therefore necessitates a rising motion west of the PV anomaly and a sinking motion east of the PV anomaly. In this way, the new convection develops upfront of the middle or upper-level PV anomaly, as seen on day −13 in Fig. 3.

c. PV inversion

The PV framework has two main properties: conservation and invertibility. The former property is the Lagrangian conservation of PV. The latter invertibility principle is that PV, once calculated by wind and temperature fields, can be inverted to produce the corresponding mass and wind anomalies under proper large-scale geostrophic and hydrostatic balance relations. Therefore, it is useful in quantitatively diagnosing the effects of PV anomalies located at different levels. Recently, the PV invertibility principle is proved valid even in the tropical regions in relation to the MJO by Schubert and Masarik (2006). We applied the PV inversion method to the three-dimensional PV anomalies from the surface up to 50-hPa level regressed against the OLR index. Figure 6a shows the streamfunction anomaly fields at 5°S derived from this inversion. Associated with the positive tropospheric PV anomaly in the Southern Hemisphere, the negative streamfunction (or positive geopotential height) anomaly appears throughout the troposphere with its shape roughly following the PV pattern (Fig. 6a). Localized peaks appear in the middle troposphere and at the lowest level.

The balanced zonal winds are predominantly easterlies with the midtropospheric peak located below the longitude of the maximum PV anomaly (~80°E) (not shown). The magnitude of the balanced lower-level winds over the Indian Ocean ranges from 0.2 to 1.0 m s^{-1} (Fig. 6b), which is about the same magnitude as the observation (Fig. 4c). An interesting feature related to this is that the wind or streamfunction response to the PV anomaly mainly occurs across the forcing longitudes and to the west of the forcing region, consistent with the recent study of Schubert and Masarik (2006), where they showed that simple PV dynamics can accurately describe the Rossby wave–related flow in the wake of an MJO convective envelope but cannot describe the Kelvin wave flow pattern ahead of it.

The wind convergence calculated with the zonal wind (Fig. 6b) demonstrates that the convergence (divergence) takes place to the west (east) of the PV anomaly center, similar to the observation. Even two convergence zones to the west of it appearing in the observation are also reproduced. The right convergence is slightly stronger than the left one, but the western convergence zone is the nominal BSISO convection initiation region because

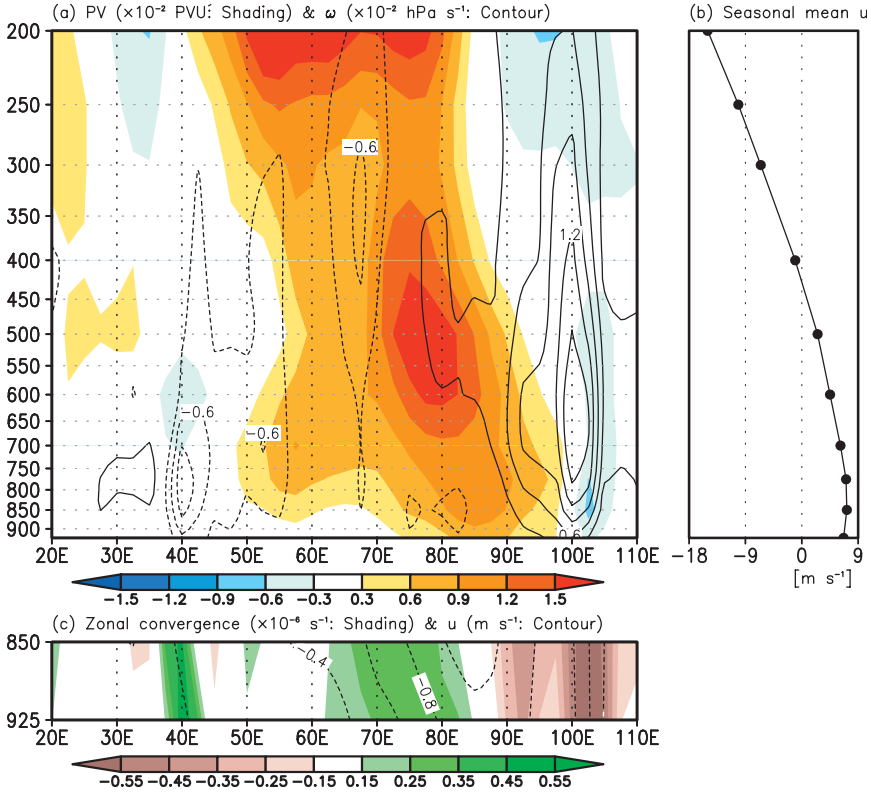

FIG. 4. Day −13 longitude–height cross sections of (a) PV (shading) and pressure velocity (contours) anomalies, (b) climatological mean zonal wind (m s^{-1}), and (c) zonal wind (contours) and wind convergence (shading) anomalies at 5°S. The intervals of PV, pressure velocity, zonal wind, and wind convergence anomalies are 0.3 × 10^{-2} PVU, 0.3 × 10^{-2} hPa s^{-1}, 0.2 m s^{-1}, and 0.1 × 10^{-5} s^{-1}, respectively.

frictional convergence due to the African continent is added to the balanced winds (because the PV inversion does not take the topographic effect into account) and topographic lifting further enhances the vertical updraft (cf. a detailed analysis will be reported in the future). All these imply that the PV anomalies in the mid troposphere can contribute to the formation of the lower-tropospheric wind anomalies.

To quantify contributions from the PV anomalies at different levels, a piecewise PV inversion method (e.g., Davis and Emanuel 1991) is applied to a PV anomaly at each level. The inversion technique is based on linear dynamics so that the summed results from PV forcing at different levels are the same as those forced from the total PV anomaly. As previously shown, the lower-level wind anomalies can be affected by the PV forcing aloft, so we calculated the contribution of the 925-hPa circulation anomalies induced by PV forcing at each level. Figure 7 shows the fractional percentage of 925-hPa streamfunction and zonal wind anomalies induced by the PV anomaly at each level at 5°S, relative to the 925-hPa streamfunction and zonal wind anomalies generated from the total PV forcing. Immediately, we can see that the significant circulation anomalies are generated from the levels higher than the 925-hPa level. About 50% of the low-level circulation variations result from PV forcing from 700 to 450 hPa. The largest contributions of about 30% are made by the 600–650-hPa PV forcing for the convection initiation WEIO region and by the 850-hPa PV forcing over the central Indian Ocean. Therefore, the lower-level wind signal necessary for the initiation of BSISO convection does not arise solely from the response to the lower-level PV forcing but from summed contribution by the PV anomalies at all levels.

Along with this dynamical environment, moisture perturbation is necessary for a new convection to occur. To show this, 925-hPa specific humidity is regressed onto the OLR index (Fig. 8). As seen in the figure, a positive moisture anomaly appears over the WEIO, whereas negative anomalies appear over the off-equatorial eastern Indian Ocean in relation to the suppressed convective anomalies there. Therefore, the new convection begins to develop under this dynamically and thermodynamically favorable environment along the eastern coast of

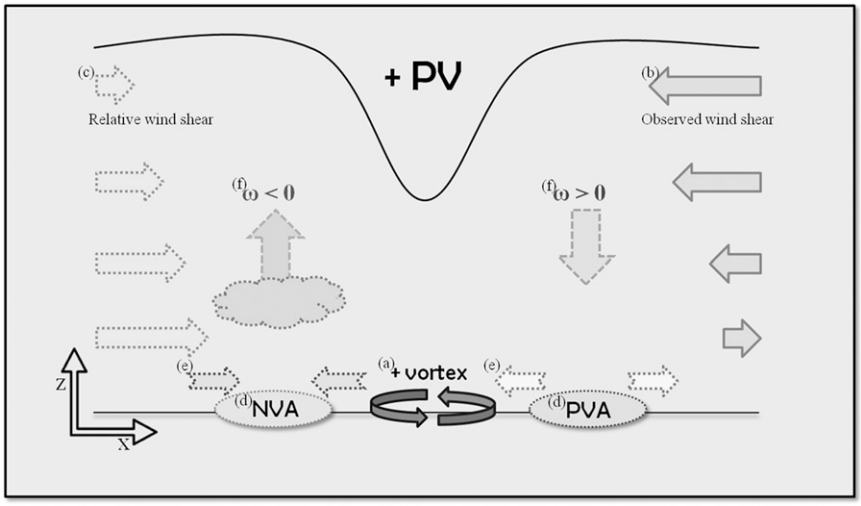

FIG. 5. Schematic diagram of the dynamical recharge mechanism for the initiation of intraseasonal convective disturbances based on PV thinking and observed characteristics. (a) The presence of the positive upper-level (upper troposphere and lower stratosphere in the extratropics and middle troposphere for the tropics) PV anomalies induces a positive vortex at the low level, and (b) the observed seasonal mean easterly zonal winds are shown as large solid arrows on the right side. (c) The relative zonal winds are shown as large dotted arrows on the left side. (d) Because of the relative zonal winds at the lower troposphere, NVA and PVA emerge west and east of the low-level positive vortex, respectively. NVA (PVA) leads to (e) the low-level convergence (divergence) and (f) midlevel upward (downward) motion. Therefore, the initiation of convective BSISO appears at the western side of the positive PV anomaly.

equatorial Africa. This moisture anomaly preconditions the atmosphere for the later flare up of deep convection (e.g., Seo and Kim 2003; Benedict and Randall 2007) by increasing the boundary layer moist static energy and potential instability.

4. Discussion

The results of this study can be compared with and incorporated into the following previously proposed theories on the initiation of the BSISO (or broadly the MJO):

(i) Discharge–recharge process: A discharge–recharge cycle of local convective instability regulates the time interval between the initiation and termination of the MJO (Bladé and Hartmann 1993). A gradual buildup of moist convective instability at the lower troposphere precedes a burst of deep convection. After the intense deep convective process (i.e., the rapid discharge phase) (Kemball-Cook and Weare 2001; Benedict and Randall 2007), the convection-free phase (recharge) prevails for some period. During this period, the sea surface warms up and convective instability increases. Consequently, the recharge phase is determined by the radiative and thermodynamic contributions at the surface and low level. The question, therefore, arises as to whether there is any dynamical recharge mechanism during this period. It is the midtropospheric PV anomaly formed by the quiescent phase (suppressed convective phase) that regulates the dynamically consistent variations vertically. As Hsu and Lee (2005) indicated, the suppressed or enhanced MJO convection over the Indian Ocean moves very slowly, exhibiting a quasi-stationary behavior. The slower the propagation within the Indian Ocean, the longer and stronger the effects of the middle-level PV anomaly will be on the atmospheric circulation over the WEIO, leading to an increased low-level moisture convergence and upward motion to the west of the PV anomaly center under the easterly basic wind shear. Therefore, this PV anomaly acts as a local dynamical recharger for the initiation of a new boreal summer intraseasonal event in the Indian Ocean.

(ii) Low-level convergence mechanism: The frictional convergence mechanism is the prevailing dynamic paradigm for the development and maintenance of the MJO (Wang 1988; Salby et al. 1994; Maloney and Hartmann 1998). At the initiation phase of the BSISO (Fig. 4b), which arises over the WEIO along the eastern coast of Africa, the significant moisture convergence occurs because of the perturbation easterly wind (Seo and Kim 2003; Annamalai and Sperber 2005). Basically, the convergence zone is

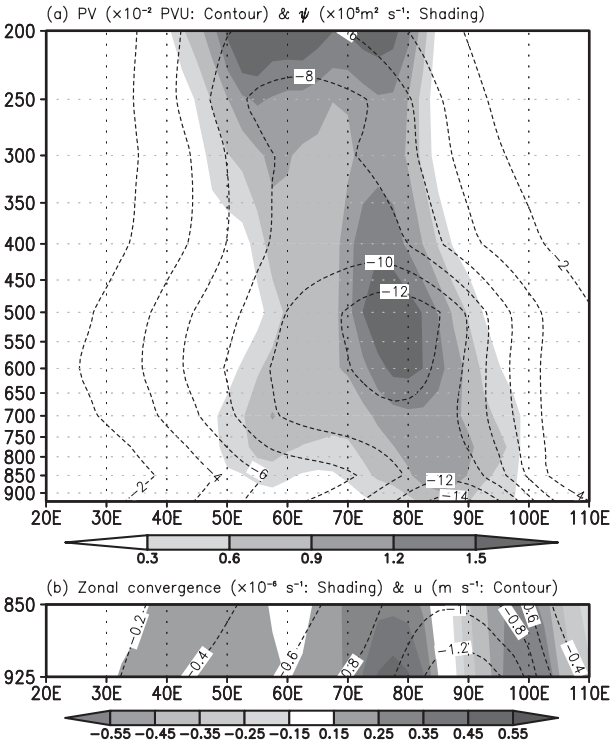

FIG. 6. Longitude–height cross sections of derived circulation fields at 5°S from the PV inversion. (a) PV anomaly (shading) and derived streamfunction anomaly (contours) and (b) derived zonal wind anomaly (contours) and wind convergence anomaly (shading). The PV anomaly is as in Fig. 4a. The intervals of PV, streamfunction, zonal wind, and wind convergence anomalies are 0.3×10^{-2} PVU, 2×10^5 s^{-1}, 0.2 m s^{-1}, and 0.1×10^{-5} s^{-1}, respectively.

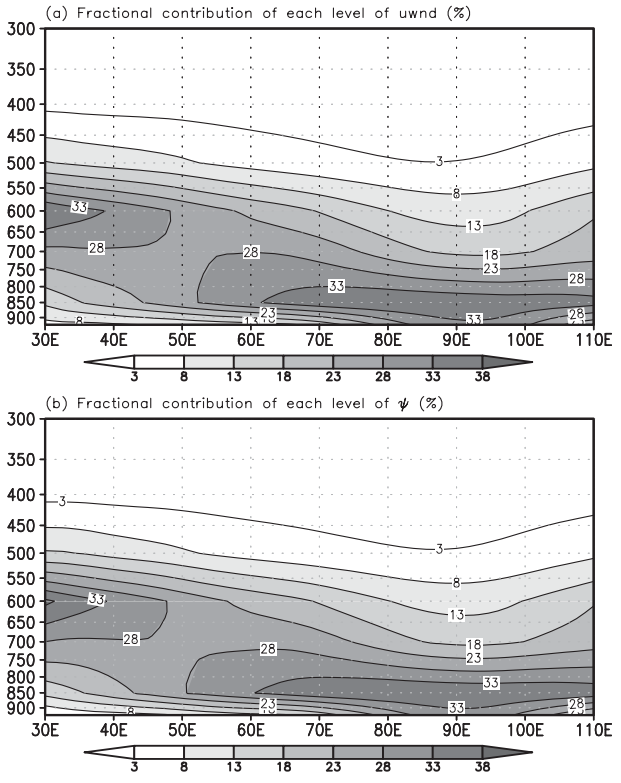

FIG. 7. Fractional percentage (%) of 925-hPa (a) streamfunction and (b) zonal wind anomalies induced by PV forcing at each level, relative to the 925-hPa streamfunction and zonal wind anomalies induced from the total PV forcing at 5°S. The intervals are shown on the gray scale.

formed by a dramatic change of the anomalous winds between the ocean and the African landmass. The applied PV thinking is similar to the low-level convergence paradigm in that the midtropospheric PV act as a dynamic forcing that ultimately enhances the low-level convergence to the west.

For the temperature advection process proposed by Jiang and Li (2005), the meridional warm advection of the seasonal mean temperature gradient by the BSISO wind and of the perturbation temperature gradient by the seasonal mean wind is responsible for the low-level convergence and the formation of a positive specific humidity anomaly over the WEIO. In contrast, the current study appears to indicate that the zonal temperature advection by the easterly zonal wind from the warm pool region to the WEIO is a more dominant process. However, this study still supports a self-sustained oscillation concept in the tropical Indian Ocean.

(iii) Upstream wave effect: Low-level circulation anomalies induced by the previous cycle of the MJO tend to circumnavigate eastward along the equator as Kelvin waves (Seo and Kim 2003; Hsu and Lee 2005). As shown in Fig. 9a, by day −19 the negative 1000-hPa geopotential height anomaly has already arrived in Africa, thereby producing a zonal pressure gradient between Africa and the WEIO (Hsu and Lee 2005; Ray et al. 2009). This tends to strengthen the easterly wind anomaly further at a later time (Fig. 9b), implying that the encircling Kelvin wave mere plays a secondary role in initiating the convection. However, any upstream in situ Kelvin wave forcing as presented by Hsu and Lee (2005) is not seen in this BSISO case.

(iv) Extratropical influence: Extratropical intraseasonal or high-frequency perturbations are proposed as a trigger mechanism for the MJO (Lau and Peng 1987; Hsu et al. 1990; Lin et al. 2007; Matthews 2008; Ray and Zhang 2010). To find such a possibility, the wave activity flux has been estimated as done by Ray and Zhang (2010) (not shown). This vector represents the propagation of a packet of wave disturbances, thereby making it possible to infer the source and sink of the wave packet. The maps of

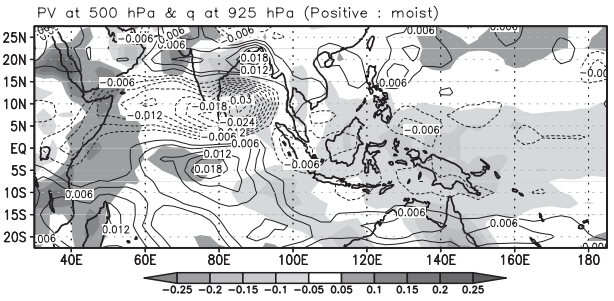

FIG. 8. Horizontal field of 925-hPa specific humidity (shading) regressed onto the OLR index at the initiation phase (day −13). The 500-hPa PV anomaly (contours) is overlaid. The intervals of PV and specific humidity are 0.3×10^{-2} PVU and 0.05 g kg^{-1}, respectively. The shaded and contoured anomalies are significant at the 90% confidence level.

wave activity flux from day −30 to day −13 regressed onto our OLR index over the Indian Ocean show no evidence of strong wave activity from the midlatitudes toward the tropics before the initiation of a BSISO event. The wave activity vectors are smallest across the equator, and the correlations with the OLR index in the region of [20°S, 20°N] are less than 0.05. Furthermore, the zonal momentum flux at the lower level is also investigated (not shown) but no significant signal is found for the initiation of the BSISO. Therefore, the climatological statistics do not indicate any explicit connection between the extratropics and the tropical convection initiation over the WEIO. Again, although the incursion of the extratropical Rossby wave into the tropics may induce a new convection over this region in an intermittent manner (Hsu et al. 1990; Ray and Zhang 2010), the systematic, periodic influence on the intraseasonal time scale cannot be established.

In addition, the climatological mean zonal winds in the boreal summer are the easterlies, so that, according to Rossby wave theory (Hoskins and Ambrizzi 1993), efficient penetration of extratropical disturbances into the deep tropics is not expected to be possible. Furthermore, the fact that somewhat significant high-frequency wave kinetic energy over the Indian sector [10°–30°N, 60°–90°E] appears at 200 hPa prior to the MJO initiation (Matthews 2008) does not actually guarantee the prominent wave propagation from the extratropics to the tropics or the triggering of the convection.

5. Summary

The initiation of the BSISO was investigated using OLR and ERA-40 data. The PV framework, initially proposed by Hoskins et al. (1985) for application to the midlatitude weather phenomena associated with cyclogenesis, cutoff lows, and cold surge, was employed as the main diagnostic tool. Because PV itself is involved in the derivative of the wind field, the information on the current atmospheric state obtained using PV is more

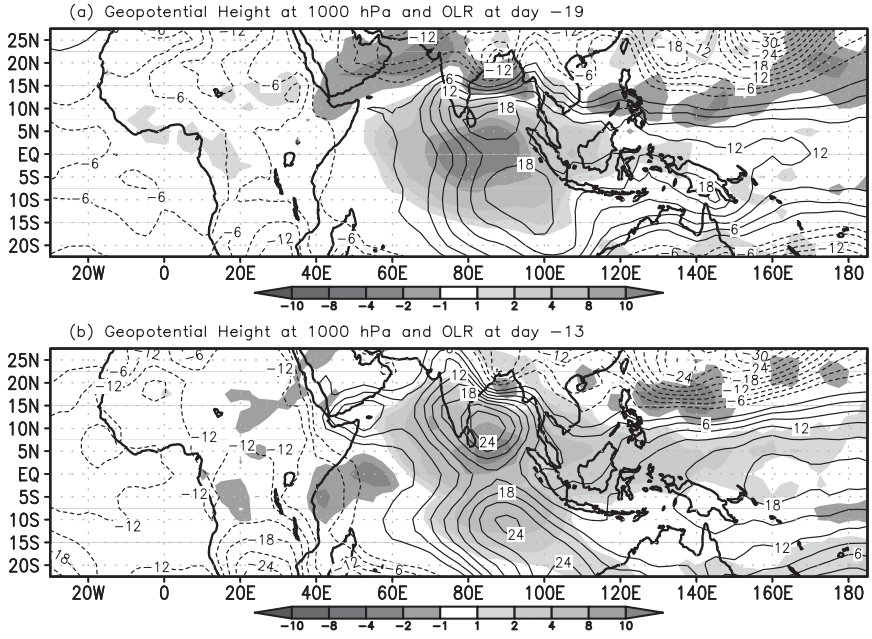

FIG. 9. Horizontal distribution of geopotential height at 1000 hPa (contours) and OLR (shading, in units of W m^{-2}) on days (a) −19 and (b) −13. The contour interval is 3 m.

detailed than that obtained using a conventional geopotential or pressure map.

Potential vorticity (PV) thinking conceptually connects the upper-level (upper troposphere and lower stratosphere in the extratropics and middle troposphere for the tropics) dynamical process to the lower-level process. We demonstrate that the midtropospheric PV anomaly produces a dynamical environment favorable for the BSISO initiation. Under seasonal easterly vertical wind shear, the PV anomaly helps enhance low-level convergence and upward motion at its western edge. Recently, Schubert and Masarik (2006) showed the validity of PV inversion even in the tropical region. Tropical PV forcing in the middle troposphere produces balanced mass and circulation fields that spread horizontally and vertically so that its effect can reach even the lowest troposphere. The downward influence of the midtropospheric PV forcing is one of the key aspects of the PV thinking. Direct piecewise PV inversions confirm that the anomalous lower-level zonal wind and its convergence necessary for the initiation of BSISO convection do not arise solely from the response to the lower-level PV but from the summed contribution by the PV anomalies at all levels. About 50% of the low-level circulation variations result from PV forcing from 700 to 450 hPa. The largest contributions of about 30% are made by the 600–650-hPa PV forcing for the convection initiation region and by the 850-hPa PV forcing over the central Indian Ocean.

The PV approach proposed here also holds for the boreal winter season, because the basic wind field in this season also exhibits easterly vertical shear. Whereas the convection initiation region in the boreal summer is the far western Indian Ocean, the boreal winter convection initiation appears ~10° east of it, possibly because the encircled Kelvin wave signature in the surface pressure forced by the previous MJO cycle has advanced farther east or perhaps because of some additional Kelvin wave forcing by in situ diabatic heating over the Africa landmass (not shown; see Hsu and Lee 2005). In addition, the climatological MJO intensity is greater in the boreal winter than in the boreal summer. The SST difference is another possible factor, but a detailed investigation is needed to determine the exact causes.

Finally, there is a lack of systematic in situ observations in the tropical Indian Ocean region, and this has hindered progress on the study of MJO or BSISO. A coordinated international field program such as the Cooperative Indian Ocean Experiment on Intraseasonal Variability in Year 2011 (CINDY2011) and Dynamics of the MJO (DYNAMO) will be implemented from October 2011 to March 2012 with the aim of elucidating deep convection initiation. The analysis of the collected local observation data is expected to improve our understanding of MJO or BSISO initiation processes.

Acknowledgments. The authors are grateful to Dr. B.-M. Kim at the Korea Polar Research Institute for assisting in employing the PV inversion technique and to Dr. Chidong Zhang for his insightful comments. We would also like to thank the three anonymous reviewers for their critical and constructive comments. This work was funded by the Korea Meteorological Administration Research and Development Program under Grant CATER 2012-3071 and the National Research Foundation of Korea (NRF) Grant 2011-0015486 from the Ministry of Education, Science and Technology. The authors acknowledge the support of the Korea Institute of Science and Technology Information (KISTI).

REFERENCES

Allen, G., G. Vaughan, D. Brunner, P. T. May, W. Heyes, P. Minnis, and J. K. Ayers, 2009: Modulation of tropical convection by breaking Rossby waves. *Quart. J. Roy. Meteor. Soc.,* **135,** 125–137.

Annamalai, H., and K. R. Sperber, 2005: Regional heat sources and the active and break phases of boreal summer intraseasonal (30–50 day) variability. *J. Atmos. Sci.,* **62,** 2726–2748.

Benedict, J. J., and D. A. Randall, 2007: Observed characteristics of the MJO relative to maximum rainfall. *J. Atmos. Sci.,* **64,** 2332–2354.

Bladé, I., and D. L. Hartmann, 1993: Tropical intraseasonal oscillations in a simple nonlinear model. *J. Atmos. Sci.,* **50,** 2922–2939.

Bluestein, H. B., 1993: *Observations and Theory of Weather Systems*. Vol. 2, *Synoptic-Dynamic Meteorology in Midlatitudes,* Oxford University Press, 608 pp.

Davis, C. A., 1992: Piecewise potential vorticity inversion. *J. Atmos. Sci.,* **49,** 1397–1411.

——, and K. A. Emanuel, 1991: Potential vorticity diagnostics of cyclogenesis. *Mon. Wea. Rev.,* **119,** 1929–1953.

Duchon, C. E., 1979: Lanczos filtering in one and two dimensions. *J. Appl. Meteor.,* **18,** 1016–1022.

Ebisuzaki, W., 1997: A method to estimate the statistical significance of a correlation when the data are serially correlated. *J. Climate,* **10,** 2147–2153.

Hendon, H. H., 1988: A simple model of the 40–50 day oscillation. *J. Atmos. Sci.,* **45,** 569–584.

Holton, J. R., 2004: *Introduction to Dynamic Meteorology*. 4th ed. Elsevier Academic Press, 535 pp.

Hoskins, B. J., and T. Ambrizzi, 1993: Rossby wave propagation on a realistic longitudinally varying flow. *J. Atmos. Sci.,* **50,** 1661–1671.

——, M. E. McIntyre, and A. W. Robertson, 1985: On the use and significance of isentropic potential vorticity maps. *Quart. J. Roy. Meteor. Soc.,* **111,** 877–946.

Hsu, H. H., and M. Y. Lee, 2005: Topographic effects on the eastward propagation and initiation of the Madden–Julian oscillation. *J. Climate,* **18,** 795–809.

——, B. J. Hoskins, and F. F. Jin, 1990: The 1985/86 intraseasonal oscillation and the role of the extratropics. *J. Atmos. Sci.,* **47,** 823–839.

——, C. H. Weng, and C. H. Wu, 2004: Contrasting characteristics between the northward and eastward propagation of the

intraseasonal oscillation during the boreal summer. *J. Climate,* **17,** 727–743.

Jiang, X. A., and T. Li, 2005: Reinitiation of the boreal summer intraseasonal oscillation in the tropical Indian Ocean. *J. Climate,* **18,** 3777–3794.

Kemball-Cook, S. R., and B. Wang, 2001: Equatorial waves and air–sea interaction in the boreal summer intraseasonal oscillation. *J. Climate,* **14,** 2923–2942.

——, and B. C. Weare, 2001: The onset of convection in the Madden–Julian oscillation. *J. Climate,* **14,** 780–793.

Kim, B.-M., J.-H. Jeong, and S.-J. Kim, 2009: Investigation of stratospheric precursor for the East Asian cold surge using the potential vorticity inversion technique. *Asia-Pac. J. Atmos. Sci.,* **45,** 513–522.

Lau, K. M., and P. H. Chan, 1986: Aspects of the 40–50 day oscillation during the northern summer as inferred from the outgoing longwave radiation. *Mon. Wea. Rev.,* **114,** 1354–1367.

——, and L. Peng, 1987: Origin of low frequency (intraseasonal) oscillations in the tropical atmosphere. Part I: The basic theory. *J. Atmos. Sci.,* **44,** 950–972.

Lin, H., G. Brunet, and J. Derome, 2007: Intraseasonal variability in a dry atmospheric model. *J. Atmos. Sci.,* **64,** 2422–2441.

Lin, J. W. B., J. D. Neelin, and N. Zeng, 2000: Maintenance of tropical intraseasonal variability: Impact of evaporation–wind feedback and midlatitude storms. *J. Atmos. Sci.,* **57,** 2793–2823.

Lin, X., and R. H. Johnson, 1996: Kinematic and thermodynamic characteristics of the flow over the western Pacific warm pool during TOGA COARE. *J. Atmos. Sci.,* **53,** 695–715.

Madden, R. A., and P. R. Julian, 1994: Observations of the 40–50 day tropical oscillation: A review. *Mon. Wea. Rev.,* **122,** 814–837.

Maloney, E. D., and D. L. Hartmann, 1998: Frictional moisture convergence in a composite life cycle of the Madden–Julian oscillation. *J. Climate,* **11,** 2387–2403.

Matthews, A. J., 2000: Propagation mechanisms for Madden-Julian oscillation. *Quart. J. Roy. Meteor. Soc.,* **126,** 2637–2651.

——, 2008: Primary and successive events in the Madden-Julian oscillation. *Quart. J. Roy. Meteor. Soc.,* **134,** 439–453.

——, and G. N. Kiladis, 1999: The tropical–extratropical interaction between high-frequency transients and the Madden–Julian oscillation. *Mon. Wea. Rev.,* **127,** 661–677.

——, B. J. Hoskins, J. M. Slingo, and M. Blackburn, 1996: Development of convection along the SPCZ within a Madden-Julian oscillation. *Quart. J. Roy. Meteor. Soc.,* **122,** 669–688.

Nong, S., and K. Emanuel, 2003: A numerical study of the genesis of concentric eyewalls in hurricanes. *Quart. J. Roy. Meteor. Soc.,* **129,** 3323–3338.

Ray, P., and C. Zhang, 2010: A case study of the mechanics of extratropical influence on the initiation of the Madden–Julian oscillation. *J. Atmos. Sci.,* **67,** 515–528.

——, ——, J. Dudhia, and S. S. Chen, 2009: A numerical case study on the initiation of the Madden–Julian oscillation. *J. Atmos. Sci.,* **66,** 310–331.

Salby, M. L., R. R. Garcia, and H. H. Hendon, 1994: Planetary scale circulations in the presence of climatological and wave induced heating. *J. Atmos. Sci.,* **51,** 2344–2367.

Schubert, W. H., and M. T. Masarik, 2006: Potential vorticity aspects of the MJO. *Dyn. Atmos. Ocean,* **42,** 127–151.

Seo, K.-H., and K.-Y. Kim, 2003: Propagation and initiation mechanisms of the Madden-Julian oscillation. *J. Geophys. Res.,* **108,** 4384–4405.

——, and A. Kumar, 2008: The onset and life span of the Madden-Julian Oscillation. *Theor. Appl. Climatol.,* **94,** 13–24, doi:10.1007/s00704-007-0340-2.

——, and W. Wang, 2010: The Madden–Julian oscillation simulated in the NCEP Climate Forecast System model: The importance of stratiform heating. *J. Climate,* **23,** 4770–4793.

——, J.-K.E. Schemm, W. Wang, and A. Kumar, 2007: The boreal summer intraseasonal oscillation simulated in the NCEP Climate Forecast System (CFS): The effect of sea surface temperature. *Mon. Wea. Rev.,* **135,** 1807–1827.

Sikka, D. R., and S. Gadgil, 1980: On the maximum cloud zone and the ITCZ over Indian longitudes during the southwest monsoon. *Mon. Wea. Rev.,* **108,** 1840–1853.

Slingo, J. M., 1998: Extratropical forcing of tropical convection in a northern winter simulation with the UGAMP GCM. *Quart. J. Roy. Meteor. Soc.,* **124,** 27–51.

Straub, K. H., and G. N. Kiladis, 2003: The observed structure of convectively coupled Kelvin waves: Comparison with simple models of coupled wave instability. *J. Atmos. Sci.,* **60,** 1655–1668.

Thayer-Calder, K., and D. A. Randall, 2009: The role of convective moistening in the Madden–Julian oscillation. *J. Atmos. Sci.,* **66,** 3297–3312.

Wang, B., 1988: Dynamics of tropical low-frequency waves: An analysis of the moist Kelvin wave. *J. Atmos. Sci.,* **45,** 2051–2065.

——, and H. Rui, 1990: Synoptic climatology of transient tropical intraseasonal convection anomalies. *Meteor. Atmos. Phys.,* **44,** 43–61.

——, and X. Xie, 1997: A model for the boreal summer intraseasonal oscillation. *J. Atmos. Sci.,* **54,** 72–86.

Yun, K.-S., K.-H. Seo, and K.-J. Ha, 2008: Relationship between ENSO and northward propagating intraseasonal oscillation in the east Asian summer monsoon system. *J. Geophys. Res.,* **113,** D14120, doi:10.1029/2008JD009901.

Zhang, C., 2005: Madden-Julian oscillation. *Rev. Geophys.,* **43,** RG2003, doi:10.1029/2004RG000158.

——, and J. Ling, 2012: Potential vorticity of the Madden–Julian oscillation. *J. Atmos. Sci.,* **69,** 65–78.